1-28-2016

Dynamic Phase-Control of a Rising Sun Magnetron Using Modulated and Continuous Current

Sulmer Fernandez-Gutierrez
Intel Corporation

Jim Browning
Boise State University

Ming-Chieh Lin
Hanyang University

David N. Smithe
Tech-X Corporation

Jack Watrous
Confluent Sciences, LLC

Dynamic phase-control of a rising sun magnetron using modulated and continuous current

Sulmer Fernandez-Gutierrez,[1,a)] Jim Browning,[2] Ming-Chieh Lin,[3] David N. Smithe,[4] and Jack Watrous[5]

[1]*Intel Corporation, 2111 NE 25th Ave, Hillsboro, Oregon 97214, USA*
[2]*Department of Electrical and Computer Engineering, Boise State University, Boise, Idaho 83725, USA*
[3]*Department of Electrical and Biomedical Engineering, Hanyang University, Seoul 133-791, South Korea*
[4]*Tech-X Corporation, 5621 Arapahoe Ave, Boulder, Colorado 80303, USA*
[5]*Confluent Sciences, LLC, Albuquerque, New Mexico 87111, USA*

Phase-control of a magnetron is studied via simulation using a combination of a continuous current source and a modulated current source. The addressable, modulated current source is turned ON and OFF at the magnetron operating frequency in order to control the electron injection and the spoke phase. Prior simulation work using a 2D model of a Rising Sun magnetron showed that the use of 100% modulated current controlled the magnetron phase and allowed for dynamic phase control. In this work, the minimum fraction of modulated current source needed to achieve a phase control is studied. The current fractions (modulated versus continuous) were varied from 10% modulated current to 100% modulated current to study the effects on phase control. Dynamic phase-control, stability, and start up time of the device were studied for all these cases showing that with 10% modulated current and 90% continuous current, a phase shift of 180° can be achieved demonstrating dynamic phase control. © 2016 AIP Publishing LLC.
[http://dx.doi.org/10.1063/1.4940376]

I. INTRODUCTION

Phase locking of magnetrons is a technique used to control the magnetron oscillation and is also used to take advantage of magnetrons that operate at lower powers. These magnetrons can be synchronized together and can be "phase locked" to a desired phase with the objective of getting a higher total power output at potentially lower cost. Phase locking is used in many applications[1–5] ranging from radar systems to materials processing. The idea is to minimize cost, to take advantage of lower power devices, and to achieve high efficiency. Phase locking has been studied since World War II with the works of Adler[6] and David.[7] The condition for locking is known as Adler's condition and is written as[6]

$$\sqrt{\frac{P_D}{P_O}} \geq 2Q \left| \frac{\omega_D - \omega_o}{\omega_o} \right|, \tag{1}$$

where P_D is the magnitude of injected power, P_O is the oscillator's output power, ω_D is the frequency of the injected signal, ω_o is the free running oscillator's resonant frequency, and Q is the quality factor of the oscillator. Because magnetrons are free running oscillators, the phase drifts over time; hence, the current phase control methods use external locking systems or gridded cathodes. Because of the power required to drive magnetrons into phase, these systems have a reduced efficiency, and they can be complicated and expensive. Therefore, there is a need to develop a new method for phase control of magnetrons that can take advantage of their high efficiency. The simulation work presented

in this work will not cover phase control of multiple magnetrons, which is a technique broadly covered in the literature;[1–5,8–14] while it will focus on the phase control of the oscillations of a single magnetron device by using a combination of a modulated, addressable, controlled electron source[15,16] and a continuous current source.[17]

The proposed device is a ten-cavity, rising sun magnetron.[18–20] As was shown in previous work,[15–17] this device is comprised of a faceted cathode with addressable current sources that allow the control of the current in time and space. These sources could be gated field emission arrays or even photocathodes. The temporal modulation of the sources allows the control of the current injection at the magnetron frequency and can be used to control the RF phase of the magnetron by controlling the electron spoke formation. This work presents a 2D simulation of the magnetron, which is accurate enough to study the device operation, mode separation, and other variables of magnetron performance. The rising sun geometry can be easily modeled in 2D which greatly reduces computation time, and it does not require a complex magnetron model such as the strapped magnetron which can only be modeled in 3D simulations. A complete 3D simulation of this magnetron is left for future work.

A 2D simulation of the faceted magnetron using the electromagnetic (EM) particle-in-cell (PIC) code VORPAL[15–17,21] demonstrated reduced start-up time and dynamic phase control when utilizing 100% modulated current. Additional simulations showed that if 90% of the current was modulated, the phase control was still maintained.

The present work analyzes the use of a much smaller fraction of modulated current by simulating the magnetron with a mixture of modulated and continuous current. The use

a)Electronic mail: sulmer.a.fernandez.gutierrez@intel.com

119, 044501-1

of a greater fraction of continuous current would reduce the current density demand on the modulated current source allowing for hybrid cathodes using a combination of the modulated cathode and either thermionic or secondary emitting cathodes, and controlling the phase using a lower modulated current requirement is highly desirable. The simulations were run for a range of modulated current from 100% down to 1% of the total current. In the best case, only 10% modulated current was needed to demonstrate phase control at start-up and to demonstrate active RF phase control to generate a phase shift of 180°. The simulation setup and results of the phase control simulations are presented here.

II. MODELING AND SIMULATION SETUP

The EM PIC code VORPAL is used to model a ten cavity, rising sun magnetron with a ten-sided faceted cathode in 2-D. The geometry and dimensions of the cathode are discussed in detail elsewhere.[15,17] This device oscillates at 957 MHz; for the 2D simulation, it has a loaded cavity which acts as an absorber to simulate the RF power dissipation in the device as well as to tune the quality factor. Figure 1 shows the rising sun magnetron geometry in the VORPAL simulation with 10 cavities and with the 5 electron spokes of the π-mode. As can be seen, the cavities are of two different lengths. For the standard simulation case, the operating parameters were set up as follows: a cathode-anode voltage (V_{ca}) of -22.2 kV, applied magnetic field (B) of 0.09 T, and a total linear emitted current density (J'_e) of 326 A/m. The typical linear power density is 1.2 MW/m. For this new work, a quality factor, Q = 202, was used. In the prior work, Q = 400 was used, but it is lowered here to be more in line with operating magnetrons. This device has a faceted cathode with ten facet plates. As was demonstrated via simulation,[15] the device has five electron spokes operating in the π-mode, and because the rising sun magnetron operates in
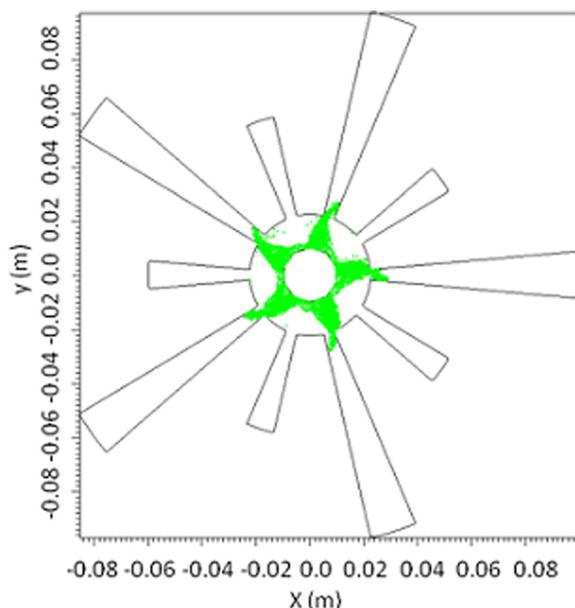
the π-mode as its primary mode, strapping was not required, thus allowing 2D simulations. The simulation was set up in VORPAL using Cartesian coordinates (x,y) with a spatial grid of 202×202. The time step size was set to1 ps, and the total run time was set to 200 ns. These simulation parameters were based on the previous work.[15–17]

Each facet contains 3 emitter elements, which can be turned ON and OFF at any desired time. In the simulation, electrons are injected as either modulated or continuous. In the modulated case to control the phase, electrons are turned ON simultaneously at five different emitter elements located symmetrically around the cathode to inject current for the five spokes of the π-mode. With ten facets and five spokes, two facets (six emitter elements) control one spoke. Hence, all six emitter elements over two facets are turned ON and OFF over one RF period with five symmetrically placed elements ON at any one time. These elements are then turned ON and OFF in 1/6th of an RF period, and the five adjacent emitter elements are then turned ON and OFF sequentially to match the rotation of the spokes. Details of this technique were previously described.[16]

III. RESULTS AND DISCUSSION

A. Combination of modulated current and continuous current

The objective of this new work was to achieve phase control of the magnetron using the smallest fraction of modulated current possible while still maintaining stability of the oscillation. The percentage of modulated current was varied from 1% to 100% to allow for a range of comparisons in terms of start-up time of oscillation, spoke stability, and phase control. Figure 2 shows the electron spokes at 159 ns
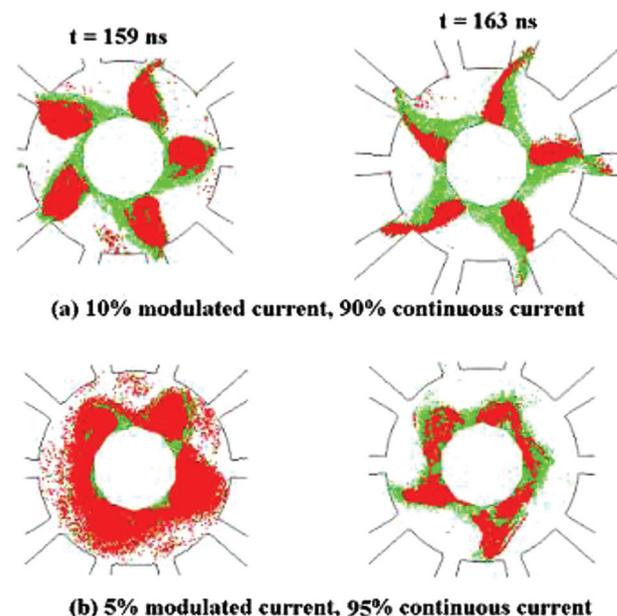

FIG. 2. Ten-sided faceted cathode with both a modulated, addressable current source (red particles) and a continuous current source (green particles). The red particles are brought forward in the image and cover the green particles. (a) 90% continuous current (green electrons) fraction and a 10% modulated current (red particles) fraction. (b) 95% continuous current (green electrons) fraction and a 5% modulated current (red particles) fraction.

FIG. 1. Rising sun magnetron geometry in the VOPRAL simulation showing five electron spokes.
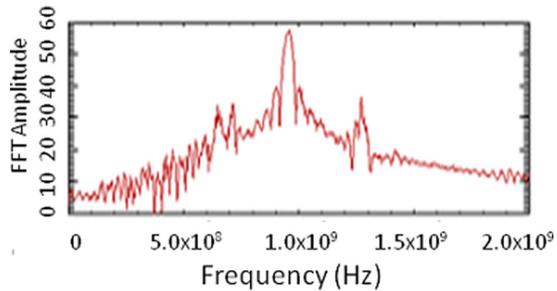
FIG. 3. Fast Fourier transform (FFT), over entire simulation time, for 10% modulated current and 90% continuous current, of the loaded cavity voltage from VORPAL simulation. This plot indicates that the π-mode is dominant at the frequency of operation of 957 MHz.

and 163 ns, after start of oscillation, from the VORPAL simulation using (a) 10% modulated current and 90% continuous current and (b) 5% modulated current and 95% continuous current. The green dots represent the electrons for the fraction of continuous current, and the red dots represent the electrons for the fraction of modulated current. These images are meant to be representative of the spoke appearances during the simulations. This simulation was run for 200 ns to make sure the model was stable over time. As can be observed, the device shows clear electron spokes and π-mode operation with the 5 spokes for the 10% modulated current and 90% continuous current case. The continuous current electrons have been pulled into the electron spokes along with the modulated current electrons. However, at 5% modulated current, the magnetron was unstable and did not oscillate consistently. This can be seen where the spokes are not properly formed and are not reaching the anode. In addition, at the 159 ns time step, there are not even five formed spokes. This result is discussed in more detail below.

Figure 3 shows the fast Fourier transform (FFT) of the cavity voltage calculated over the entire simulation run time for the 10% modulated current case. The device oscillates at 957 MHz, as expected from all previous models.[16,17] Figure 4 shows the loaded cavity voltage frequency versus time. From this plot and from the spoke formation in the simulation, the start-up time for this case is estimated to be $\approx$145 ns as indicated in the plot. This estimate method is used in our prior work. Using this same approach, the start-up times were estimated for different fractions of modulated current.

Figure 5 shows the start-up time versus the ratio of modulated current to total current (modulated plus continuous). From this curve, it can be observed that when the
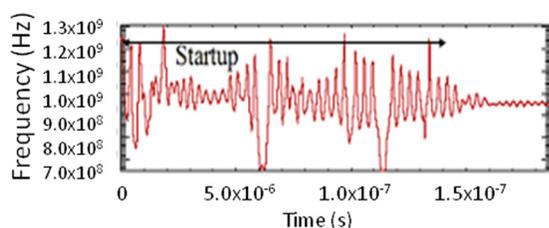

FIG. 4. Cavity voltage frequency versus time with moving window, showing the startup time of the device at ~145 ns showing the operating frequency (π-mode) at 957 MHz for 10% modulated current and 90% continuous current from VORPAL.
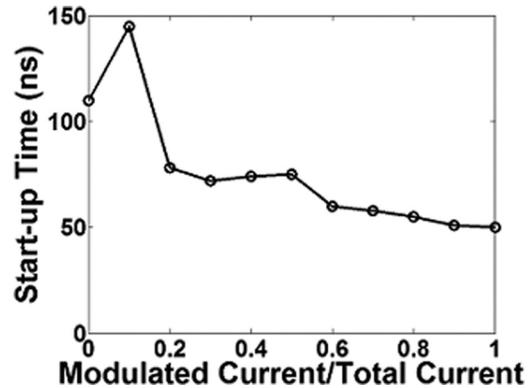

FIG. 5. Startup time versus the ratio of modulated current to total current.

device is operated with 100% continuous current the startup time is 110 ns, and when it is operated at 100% modulated current, the device start up time is reduced to 50 ns as described in our prior work. As a function of the current ratio, the start-up time first increases from 110 ns at 0% modulated current to 145 ns at 10% modulated current; then the start-up time decreases sharply dropping to $\approx$75 ns at 20% modulated current. Above 20% modulated current, the start-up time decreases monotonically to that of the 100% modulated current case. This result from 20% to 100% modulated current is expected as the injection of modulated current controls spoke formation and drives the magnetron to oscillation more quickly than with random start-up. The greater the fraction of current that is injected "in phase," the sooner oscillation will start. Below 20% modulated current, the results are more complicated. As the modulated current fraction decreases, the continuous current begins to dominate the start-up and oscillation. At 5% modulated current, the simulation did not show stable oscillations as described above. It is believed that the modulated current tries to initiate spoke formation out of phase with the always random oscillations being initiated by the continuous current. Hence, these two sources compete and prevent stable oscillation. It is possible that if the simulation was run for a long enough time, the device would eventually oscillate at the modulated current phase. At 10% modulated current, the magnetron starts later than for 0% modulated current as it again appears that the continuous current source tries to oscillate out of phase. This results in the longer start-up time. These results indicate that the modulated electrons compete with the continuous current electrons to control the oscillation start-up.

The efficiency of the magnetron has been shown to improve by use of the modulated current technique.[16] The power and efficiency for the 10% modulated case were calculated for comparison with the 100% modulated case and the 0% modulated case. Table I shows a summary of results of the linear anode current density, the calculated input power density, the loaded cavity power, and the calculated efficiency for the modulated and continuous current source models. The cold Q (quality factor) value for this model is 202. For the case of the 10% modulation, the hot Q value for the power in Table I is approximately 154. The loaded cavity power results show that the 100% modulation technique increases the output power density and efficiency compared

TABLE I. Cavity power and efficiency for different modulation fractions. CC—continuous current and MC—modulated current.

Cathode current	Anode current density $J'a$ (A/m)	Pin (MW/m)	Loaded cavity power density (MW/m)	Efficiency η (%)
0% MC/100% CC	34.23	0.76	0.6	78.9
100% MC/0% CC	44.82	1.1	0.98	89.0
10% MC/90% CC	35.45	0.78	0.6	76.9

to the continuous current case showing an efficiency of about 89% compared to 78.9%. For the modulated case, the anode current density increases from 34.23 A to 44.82 A/m, and the output power increases to 0.98 MW/m. However, for the 10% modulated case, it is observed that the results are very similar to the continuous current source model, which is expected, since 90% of the current is continuous and is not injected in phase; this current is also returned to the cathode after circulating in the interaction space region. The gain in efficiency using this method is negligible. Note, this efficiency should not be taken as absolute value and should only be used for comparison purposes. Longitudinal losses due to the axial drifting of electrons are not considered, as well as modulation power; these could be the reasons for the high efficiency results. This is a 2D simulation, and there is no real output port; therefore, this power density is not the real coupled output power but the power generated with this loaded Q. However, these results can be used as a relative estimation of the power at the loaded cavity.

B. Active phase control using 10% modulated current and 90% continuous current

The phase control was studied for the various fractions of modulated current to find the lowest fraction for which the oscillation was stable and the phase was controlled. This result was found for 10% modulated current and 90% continuous current. To determine the RF phase stability, the RF magnetic field (B_z) from one of the cavities was analyzed versus time. After oscillation was determined to be stable, a temporal reference point was chosen, and the phase of the B_z field at later times (multiples of RF periods) was then compared to the

reference time period. From this analysis, the phase difference versus time can be determined. The result demonstrates that the RF phase difference for the 10% modulated case is constant, while the case of 100% continuous current (0% modulated) has a randomly varying phase over time. Hence, this result demonstrates that using only 10% modulated current results in phase control of the magnetron.

Active phase control with 10% modulated current was also demonstrated by changing the injection timing of the modulated current. After the oscillation had started, the emitter elements were driven 180° out of phase compared to the start-up timing. The total run time was 200 ns, and the phase shift was started at 155 ns when the system was stable. Figure 6 shows the transition of the electron spokes over time during the 180° phase change. As can be seen, the spokes move to spatial locations exactly between the starting reference locations (adjacent cavities), thus indicating the phase change. Using the phase of the RF B_z field, the phase difference with a reference time (155 ns) before the phase change initiation was calculated. Figure 7 shows this phase change versus RF periods after the initiated phase change. As can be seen, the phase shifts nearly 180° after 12 RF periods from the phase shift. There appears to be an almost asymptotic approach to full 180° shift, however. The phase shift time is dependent upon the device Q. This result clearly demonstrates that not only the phase can be controlled at start-up but also the phase can be actively controlled after oscillation starts using only 10% modulated current. Also shown in Fig. 7 is the dynamic phase shift using 100% modulated current. These results are almost identical to the 10% modulated case demonstrating that the reduction in modulation current does not appear to affect the dynamic phase control after start-up despite the longer start-up time seen in the 10% modulated case.
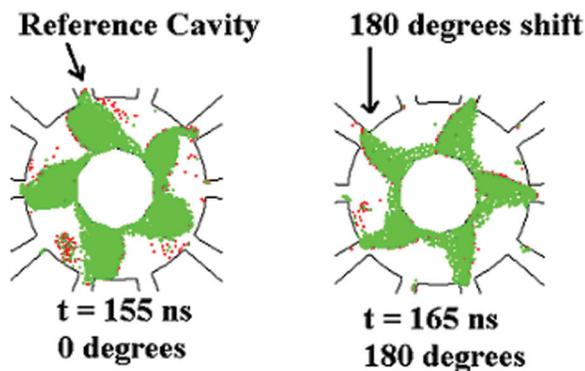

FIG. 6. Ten-sided faceted cathode with 10% modulated current and 90% continuous current, showing transition to a phase shift of 180°. Red particles are from the modulated, addressable current source and green particles are from the continuous current source. Reference Phase = 0° at 155 ns, after 10 RF periods, the electron spokes are shifted 180°.
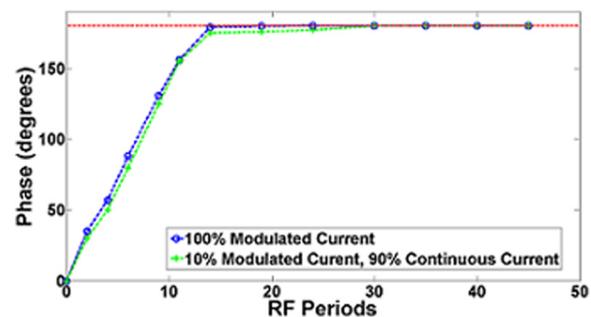

FIG. 7. VORPAL simulation results showing the change in RF phase vs. RF period for a Q = 202 after a 180° phase shift is generated using 10% modulated current and 90% continuous current and using 100% modulated current. Phase was determined from the RF B_z component.

IV. CONCLUSIONS

A ten-sided faceted cathode with a hybrid of modulated current and continuous current was simulated. This combination did not affect the operating frequency of the device. The start-up time generally decreased with increasing modulated current as expected, but the start time decreases slightly above 20% modulated current. Below 10% modulated current, the magnetron was not stable until roughly 0% modulated current. At 10% modulated current, the start-up time was the longest as the modulated current and continuous current appear to compete to control oscillation. It was demonstrated that phase can be controlled both at start-up and during oscillation with active phase control achieved with a fraction of modulated current as low as 10% of the total current. These results showed that the device can be phase controlled using a small amount of modulated current, and the rest of the current could be supplied with a continuous current source. An example of this approach might be to use a secondary emitting cathode in combination with the modulated cathode. The secondary cathode could then provide the bulk of the oscillation current. This approach would greatly reduce the current density requirements on the modulated cathode making such a system more practical and attractive. It might also be possible to place the modulated cathode at the ends of the device (near the magnetron end-hats) to keep the source away from the primary interaction space. However, the secondary current might begin to dominate oscillation and compete with the modulated current, and then phase control could be lost. The simulations presented here did not include any secondary electron emission as a byproduct of electron back-bombardment; such effects could also negatively affect the phase control. These concepts will be studied in future simulations. Power calculations show that the 10% modulated case has the efficiency and cavity power very close to the 100% continuous current case as would be expected, so the low modulation current does not offer a potential improvement in output power and efficiency as does the 100% modulated case. Obviously, cathode switching power of the modulated cathode must be included in any consistent power calculations. The efficiencies obtained in this 2D model are very high; as it was mentioned in this work the axial losses were not considered, which could be one of the reasons for these high values. However, a complete 3D model of this magnetron is left for future work.

[1] J. Zhang, X. Chen, M. Esterson, P. Lindsay, P. Burleigh, and D. Wilson, in *Proceedings of the IEEE International Conference on Plasma Science* (2006), p. 411.

[2] X. Chen, M. Esterson, and P. A. Lindsay, Proc. SPIE **2843**(47), 47–56 (1996).

[3] A. C. Dexter, G. Burt, R. G. Carter, I. Tahir, H. Wang, K. Davis, and R. Rimmer, Phys. Rev. Spec. Top. - Accel. Beams **14**(3), 032001 (2011).

[4] T. A. Treado, P. D. Brown, R. A. Bolton, and T. Hansen, "Long-pulse, high-power, phase-locked magnetron studies," in *International Microwave Symposium Digest* (IEEE, Albuqerque, NM, 1992), Vol. 1, pp. 225–228.

[5] I. M. Rittersdorf, Y. Y. Lau, J. C. Zier, R. M. Gilgenbach, E. J. Cruz, and J. W. Luginsland, Appl. Phys. Lett. **97**(17), 171502–171503 (2010).

[6] R. Adler, Proc. IRE **61**(10), 1380–1385 (1946).

[7] E. E. David, "Locking Phenomena in Microwave Oscillators," Dissertation (Research Laboratory of Electronics, Massachusetts Institute of Technology, 1948).

[8] E. J. Cruz, B. W. Hoff, P. Pengvanich, Y. Y. Lau, R. M. Gilgenbach, and J. W. Luginsland, Appl. Phys. Lett. **95**(19), 191503 (2009).

[9] E. J. Cruz, "Peer-to-Peer Magnetron Locking" Dissertation (University of Michigan, 2011).

[10] R. J. Barker, J. H. Booske, N. C. Luhmann, and G. S. Nusinovich, *Modern Microwave and Millimeter-Wave Power Electronics* (John Wiley and Sons, Inc., Piscataway, NJ, 2005).

[11] G. B. Collins, *Microwave Magnetrons* (McGraw-Hill, New York, 1948).

[12] D. French, "Investigation of Novel Configurations for High Power Microwave Generation," Dissertation (University of Michigan, 2011).

[13] J. M. Osepchuk, IEEE Trans. Microwave Theory Tech. **50**(3), 975–985 (2002).

[14] S. Y. Liao, *Microwave Electron-Tube Devices* (Prentice-Hall, 1988).

[15] J. Browning, S. Fernandez-Gutierrez, M. C. Lin, D. N. Smithe, and J. Watrous, Appl. Phys. Lett. **104**, 233507 (2014).

[16] S. Fernandez-Gutierrez, J. Browning, M. C. Lin, D. N. Smithe, and J. Watrous, J. Vac. Sci. Technol., B **33**, 031203 (2015).

[17] S. Fernandez-Gutierrez, J. Browning, M. C. Lin, D. N. Smithe, and J. Watrous, J. Vac. Sci. Technol., B **32**(6), 061205 (2014).

[18] S. Millman and A. T. Nordsieck, J. Appl. Phys. **19**(2), 156–165 (1948).

[19] N. M. Kroll and J. W. Lamb, J. Appl. Phys. **19**(2), 166–186 (1948).

[20] A. V. Hollenberg, N. Kroll, and S. Millman, J. Appl. Phys. **19**(7), 624–635 (1948).

[21] C. Nieter and J. R. Cary, J. Comput. Phys. **196**(2), 448–473 (2004).